

Evidence for a Truncated Accretion Disc in the Low Luminosity Seyfert Galaxy, NGC 7213?

A.P. Lobban¹, J.N. Reeves¹, D. Porquet², V. Braito³, A. Markowitz⁴, L. Miller⁵ and T.J. Turner⁶

¹*Astrophysics Group, School of Physical and Geographical Sciences, Keele University, Keele, Staffordshire, ST5 8EH, UK*

²*Observatoire astronomique de Strasbourg, Université Louis-Pasteur, CNRS, INSU, 11 rue de l'Université, 67000 Strasbourg, France*

³*Department of Physics and Astronomy, University of Leicester, University Road, Leicester, LE1 7RH, UK*

⁴*Center for Astrophysics and Space Sciences, University of California, San Diego, M.C. 0424, La Jolla, CA, 92093-0424, USA*

⁵*Department of Physics, University of Oxford, Denys Wilkinson Building, Keble Road, Oxford, OX1 3RH, UK*

⁶*Department of Physics, University of Maryland Baltimore County, Baltimore, MD 21250 and Astrophysics Science Division, NASA/GSFC, Greenbelt, MD 20771, USA*

Accepted by MNRAS on 4 June 2010

ABSTRACT

We present the broad-band 0.6–150 keV *Suzaku* and *Swift* BAT spectra of the low luminosity Seyfert galaxy, NGC 7213. The time-averaged continuum emission is well fitted by a single power-law of photon index $\Gamma = 1.75$ and from consideration of the *Fermi* flux limit we constrain the high energy cutoff to be $350 \text{ keV} < E_{\text{cut}} < 25 \text{ MeV}$. Line emission from both near-neutral iron $\text{K}\alpha$ at 6.39 keV and highly ionised iron, from Fe XXV and Fe XXVI, is strongly detected in the *Suzaku* spectrum, further confirming the results of previous observations with *Chandra* and *XMM-Newton*. We find the centroid energies for the emission from Fe XXV and Fe XXVI to be 6.60 keV and 6.95 keV respectively, with the latter appearing to be resolved in the *Suzaku* spectrum. From modelling, we show that the Fe XXV and Fe XXVI emission can result from a highly photo-ionised plasma, with a column density of $N_{\text{H}} \sim 3 \times 10^{23} \text{ cm}^{-2}$. A Compton reflection component, e.g., originating from an optically-thick accretion disc or a Compton-thick torus, appears either very weak or absent in this AGN, subtending < 1 sr to the X-ray source, consistent with previous findings. Indeed the absence of Compton reflection from either neutral or ionised material coupled with the lack of any relativistic Fe K signatures in the spectrum suggests that an inner, optically-thick accretion disc is absent in this source. Instead, the accretion disc could be truncated with the inner regions perhaps replaced by a Compton-thin Radiatively Inefficient Accretion Flow (RIAF). Thus, the Fe XXV and Fe XXVI emission could both originate in ionised material perhaps at the transition region between the hot, inner flow and the cold, truncated accretion disc on the order of $10^3 - 10^4$ gravitational radii from the black hole. The origin for the unresolved neutral Fe $\text{K}\alpha$ emission is then likely to be further out, perhaps originating in the optical Broad Line Region or a Compton-thin pc-scale torus.

Key words: accretion, accretion discs – atomic processes – X-rays: galaxies

1 INTRODUCTION

NGC 7213 is a nearby low-luminosity AGN ($z = 0.005839$), often classified as an intermediate between a Seyfert 1 and a LINER (Low-Ionisation Nuclear Emission-line Region) galaxy due to its optical spectrum (Filippenko & Halpern 1984). Its X-ray spectral properties also appear to lie between those of weak AGN (e.g., M81) and ‘classical’ higher-luminosity broad-line Seyferts. The ultraviolet (UV) flux measured by Wu, Boggess & Gull (1983) was higher than would be expected from an extrapolation of the optical flux, indicating that NGC 7213 may have a Big Blue Bump (BBB), although weak compared to most Seyferts. This object has a high black hole mass of about $10^8 M_{\odot}$ as estimated from the stellar velocity dispersion (Nelson & Whittle 1995; Woo & Urry 2002) and a

low bolometric luminosity (L_{bol}) of about $9 \times 10^{42} \text{ erg s}^{-1}$ (Starling et al. 2005).

NGC 7213 has a very low accretion rate of only 0.07% L_{Edd} , a value which is intermediate between those usually found in local Type 1 Seyfert Galaxies (e.g., Padovani & Rafanelli 1988; Wandel 1999; Page 2001) and LINERs (e.g., Ho 1999). Interestingly, this is much less than the predicted 2% L_{Edd} ‘critical’ rate whereby the high/soft state in black hole X-ray binaries can be observed (Maccarone 2003). Furthermore, this object exhibits another interesting characteristic since it is part of a class of Seyfert galaxies which have radio properties that are intermediate between those of radio-loud and radio-quiet active galaxies (e.g., Blank, Harnett & Jones

2005 and reference therein). It is therefore conceivable that NGC 7213 is an analogue of the Galactic low/hard state sources.

A simultaneous *XMM-Newton* (net EPIC-pn exposure ~ 30 ks) and *BeppoSAX* observation in May 2001 revealed further peculiar characteristics of NGC 7213. The low S/N RGS (Reflection Grating Spectrometer) spectrum showed the presence of several weak emission features with no absorption lines (Starling et al. 2005) contrary to what is usually found in Seyfert Type 1 Galaxies. Moreover, the emission lines appeared to be the signature of a collisionally-ionised thermal plasma ($k_B T \sim 0.18$ keV), while in Seyfert Galaxies, only emission and/or absorption lines from a photo-ionised warm absorber / emitter have before been observed (e.g., NGC 3783, Kaspi et al. 2001; NGC 4151, Schurch & Warwick 2002; NGC 1068, Kinkhabwala et al. 2002; Brinkman et al. 2002; Mrk 3, Pounds & Page 2005). Such emission lines from collisionally-ionised thermal plasma have, however, been observed in the soft X-ray spectra of LINERs, such as M81 (Page et al. 2003). Interestingly, no significant Compton reflection was observed in this simultaneous *XMM-Newton* and *BeppoSAX* observation (reflection component: $R = \Omega/2\pi < 0.2$, where a value $R = 1$ corresponds to reflection off material subtending 2π sr; Bianchi et al. 2003), though the presence of a significant Fe K complex could be explained by three narrow emission lines: neutral iron at around 6.40 keV with an EW of ~ 80 eV, Fe XXV at around 6.66 keV and Fe XXVI at about 6.94 keV (see also Starling et al. 2005).

Bianchi et al. (2003) deduced from the absence of the reflection component that the neutral iron K α emission line is most likely produced in a Compton-thin torus or the Broad Line Region (BLR). Indeed, according to Matt, Perola & Pirolo (1991) and George & Fabian (1991), a line with an EW of ~ 80 eV would require a reflection component of about $R \sim 0.6$, a larger value than that found for this object ($R < 0.2$). Furthermore, Bianchi et al. (2008) reported the data analysis of a long *Chandra*/HETG observation of NGC 7213 finding that the neutral iron K α line is resolved with a FWHM value of 2400^{+1100}_{-600} km s $^{-1}$, fully consistent with the H α line width (2640^{+110}_{-90} km s $^{-1}$) measured with the ESO/NTT telescope. They therefore inferred that the neutral Fe K line seen in this object originates in the Compton-thin BLR explaining the lack of evidence for Compton reflection. They also confirmed the presence of two ionised iron lines at ~ 6.72 keV and ~ 6.99 keV which they associate most probably with the resonance transition of the Fe XXV triplet and the Ly α transition of Fe XXVI, respectively. Comparing the line energies found with their rest-frame values, a blue-shift of about 900 km s $^{-1}$ is inferred. If the dominant line at ~ 6.72 keV is indeed the resonance line of the Fe XXV triplet, then this means that the line may be associated with a collisionally-ionised thermal plasma (Porquet & Dubau 2000; Bautista & Kallman 2000).

Here we report on a 90 ks *Suzaku* (Mitsuda et al. 2007) observation of NGC 7213. The overall goal is to understand accretion in an AGN at low rates compared to Eddington, through a high signal-to-noise, broad-band observation of this source. Specifically, the objectives are to parameterise the iron line complex with an analysis of the XIS (X-ray Imaging Spectrometer) spectra in order to constrain the individual properties of the lines before considering the complete broad-band spectra from 0.6–150 keV with a combined analysis of the *Suzaku* XIS and HXD (Hard X-ray Detector) data with that from the time-averaged *Swift* BAT 22-month survey (see Section 3). The aims are to obtain better constraints on the origin of both the iron line complex and any observed soft ex-

cess whilst simultaneously testing for the presence (or absence) of a Compton reflection component (see Section 4).

2 SUZAKU ANALYSIS AND DATA REDUCTION

2.1 Suzaku Analysis

NGC 7213 was observed by *Suzaku* on October 22 2006 with a total net exposure of 90 ks. In this paper we discuss data taken from the 4 XIS (Koyama et al. 2007) CCDs and the PIN diodes of the HXD (Takahashi et al. 2007).

Events files from version 2.0.6.13 of the *Suzaku* pipeline processing were used. All events files were screened within XSELECT to exclude data taken within the SAA (South Atlantic Anomaly) as well as excluding data with an Earth elevation angle (ELV) < 5 degrees. Data taken with Earth day-time elevation angles (DYE_ELIV) less than 20 degrees were also excluded. A cut-off rigidity (COR) criteria of > 6 GeV/c for the XIS was applied. Only good events with grades 0,2,3,4 and 6 were used, while hot and flickering pixels were removed from the XIS images using the CLEANSIS script. Time intervals affected by telemetry saturation were also removed.

Subsequently, source spectra from the XIS CCDs were extracted from circular regions of $2.3'$ radius centered on the source, in the on-axis XIS nominal pointing position. Background spectra were extracted from $2.3'$ circles offset from the source region, avoiding the calibration sources on the corners of the CCD chips. XIS response files (RMFs) and ancillary response files (ARFs) were generated using the XISRMFGEN and XISSIMARFGEN FTOOLS respectively including correction for the hydrocarbon contamination on the optical blocking filter (Ishisaki et al. 2007). A net XIS source exposure of 90.7 ks was obtained for each of the 4 XIS chips. The 3 front-illuminated XIS chips (XIS 0,2,3; hereafter XIS-FI) are predominantly used in this paper as they have the greatest sensitivity at iron K. These chips were found to produce consistent spectra within the statistical errors, so the spectra and responses were combined to maximise signal to noise. The net source count rate for the 3 XIS combined was 1.585 ± 0.002 counts s $^{-1}$ per XIS, with the background rate only 0.7% of the source rate. This count rate corresponds to an observed flux of 2.46×10^{-11} erg cm $^{-2}$ s $^{-1}$ and a luminosity of 1.85×10^{42} erg s $^{-1}$ over the 2–10 keV range. The XIS source spectrum was binned at the HWHM resolution of the detector due to the high photon statistics. This enabled the use of χ^2 minimisation as there were > 50 counts per resolution bin. Errors are quoted to 90% confidence for 1 parameter (i.e., $\Delta\chi^2 = 2.7$) unless otherwise stated.

2.2 HXD Reduction

As NGC 7213 is below the detection threshold of the HXD/GSO, we used data from the HXD/PIN only, where this object is detected at the 13σ level relative to the background. The source spectrum was extracted from the cleaned HXD/PIN events files and processed with the screening criteria described above. The HXD/PIN instrumental background spectrum was generated from a “tuned” time dependent model provided by the HXD instrument team (Fukazawa et al. 2009). Both the source and background spectra were made with identical GTIs (Good Time Intervals) and the source exposure was corrected for detector downtime (which is $\approx 6.7\%$). A detailed description of the PIN detector downtime is

given in Kokubun et al. (2007). The net exposure time of the PIN source spectrum was 84.3 ks after deadtime correction. Note that the background spectral model was generated with $10\times$ the actual background count rate in order to minimise the photon noise on the background; this has been accounted for by increasing the effective exposure time of the background spectra by a factor of $\times 10$. The HXD/PIN response file dated 2008/01/29 (epoch 3) for the XIS nominal position was used for these spectral fits.

In addition, a spectrum of the cosmic X-ray background (CXB) (Boldt 1987; Gruber et al. 1999) was also simulated with the HXD/PIN. The form of the CXB was taken as $9.0 \times 10^{-9} (E/3 \text{ keV})^{-0.29} \exp(-E/40 \text{ keV}) \text{ erg cm}^{-2} \text{ s}^{-1} \text{ sr}^{-1} \text{ keV}^{-1}$. When normalised to the field of view of the HXD/PIN instrument, the effective flux of the CXB component is $8.49 \times 10^{-12} \text{ erg cm}^{-2} \text{ s}^{-1}$ in the 15–50 keV band corresponding to a count rate of $\sim 0.017 \text{ counts s}^{-1}$. The net flux of NGC 7213 measured by the HXD over the same band is $3.58 \times 10^{-11} \text{ erg cm}^{-2} \text{ s}^{-1}$, i.e., the CXB component represents 24% of the net source flux measured by the HXD/PIN. Note that there may be some uncertainty in the absolute flux level of the CXB component measured between missions; for instance, Churazov et al. (2007) find the CXB normalisation from INTEGRAL to be about 10% higher than measured by Gruber et al. (1999) from the HEAO-1 data. However, a factor of $\pm 10\%$ uncertainty in the CXB normalisation would result in a $\pm 2.4\%$ uncertainty in the HXD flux for NGC 7213, which is well within the statistical uncertainty of the HXD/PIN observations. After background subtraction (including both the instrumental and CXB components), the resulting net PIN source count rate from 15–50 keV was $0.062 \pm 0.002 \text{ counts s}^{-1}$ corresponding to a 15–50 keV flux of $3.58 \times 10^{-11} \text{ erg cm}^{-2} \text{ s}^{-1}$. Note that the total background count rate was $\sim 0.350 \text{ counts s}^{-1}$ (15–50 keV) with a typical 1σ systematic uncertainty of $\pm 1.3\%$.

We used 0.6–10 keV data in both the XIS–FI and XIS–BI spectra. We ignored the 1.7–1.9 keV band in the co-added FI spectrum and the BI spectrum due to uncertainties in calibration associated with the instrumental Si K edge. In all fits, we included a constant multiplicative factor to account for relative instrument normalisations. We allowed the relative XIS–BI/XIS–FI normalisation to vary, but best-fit values were always within 1% of each other.

A visual analysis of the lightcurves was undertaken to determine whether any detailed timing analysis was necessary. It can be seen from Figure 1 that the amplitude of the XIS–FI lightcurve varies only by a factor of ~ 0.1 throughout the entire observation indicating little intrinsic variability below 10 keV. From Figure 2 it can be seen that the HXD/PIN lightcurve, too, shows little evidence of any substantial variability in the hard X-ray band. Therefore, due to the lack of any strong evidence of short-timescale spectral variability, we proceed to consider the time-averaged spectrum (Section 3).

3 SPECTRAL ANALYSIS

The XSPEC v11.3 software package (Arnaud 1996) was used for spectral analysis of the background-subtracted spectrum. In all fits, we included the Galactic column density ($N_{\text{H}}^{\text{Gal}} = 1.1 \times 10^{20} \text{ cm}^{-2}$, obtained from the FTOOL NH using the compilations of Dickey & Lockman 1990 and Kalberla et al. 2005) and used the cross-

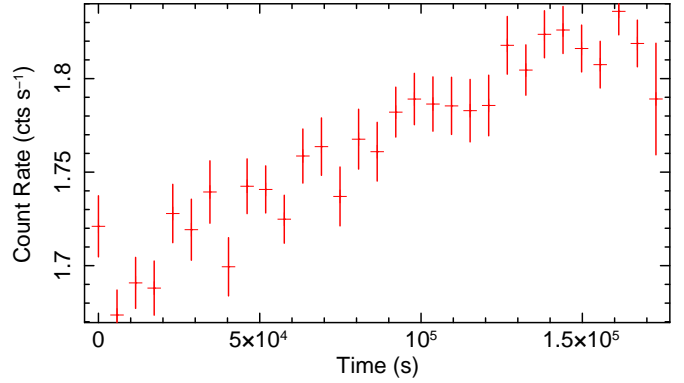


Figure 1. XIS–FI background-subtracted lightcurve of NGC 7213 from 0.5–10 keV in 5760 s orbital bins.

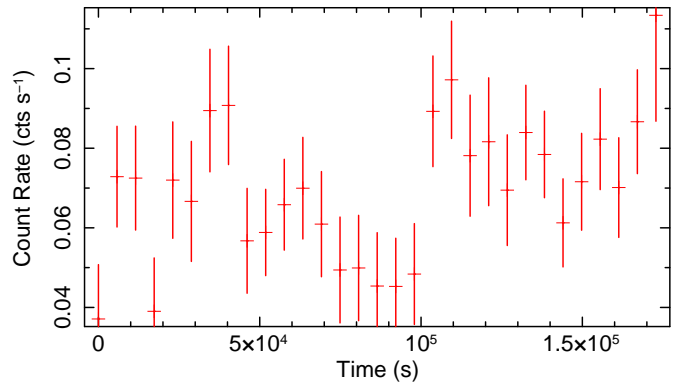


Figure 2. Net background-subtracted HXD/PIN lightcurve of NGC 7213 from 15–50 keV in 5760 s orbital bins.

sections for X-ray absorption by the interstellar medium from Morrison & McCammon (1983). Note that all fit parameters are given in the rest frame of the galaxy, assuming a distance of 25 Mpc to NGC 7213 (Mould et al. 2000). Abundances are those of Anders & Grevesse (1989) unless otherwise stated.

The cross-normalisation between the HXD/PIN and XIS detectors was accounted for by the addition of a fixed constant component at a value of 1.16 for the XIS nominal pointing position, a value derived using *Suzaku* observations of the Crab (Ishida, Suzuki & Someya 2007¹).

3.1 The Fe K line profile

The X-ray spectrum was initially analysed in the 0.6–50 keV band using both the XIS–FI and HXD/PIN data. A power-law with Galactic absorption of column density $N_{\text{H}} = 1.1 \times 10^{20} \text{ cm}^{-2}$ was fitted to the data revealing a slight soft excess at energies $< 1 \text{ keV}$ as shown in Figure 3. The XIS 1 data were included in this fit to check for consistency. For clarity, the HXD data were binned to 10σ per spectral bin relative to the background. The hard X-ray data are seen to extrapolate quite well to the XIS data with very

¹ <ftp://legacy.gsfc.nasa.gov/suzaku/doc/xrt/suzakumemo-2007-11.pdf>

Model Component	Fit Parameter	Value	χ^2/dof	$\Delta\chi^2$
1. Power-law Continuum ^a	Γ	1.75 ± 0.02		
	Normalisation	$6.25^{+0.02}_{-0.06}$		
	$F_{2.5-10 \text{ keV}}$	2.18×10^{-11}		
2. Galactic Absorption ^b	N_{H}	1.10×10^{20}	739/316	
3. Fe K α Line ^c	E_{line}	6.39 ± 0.01	422/313	316.8
	σ	$< 4.30 \times 10^{-2}$		
	EW	$83.1^{+11.0}_{-10.7}$		
	FWHM	< 4600		
	Line Flux	$2.18^{+0.28}_{-0.29}$		
4. H-like Line ^c	E_{line}	6.95 ± 0.03	365/310	57.1
	σ	$0.10^{+0.05}_{-0.04}$		
	EW	$62.3^{+16.0}_{-14.2}$		
	FWHM	10000^{+5000}_{-4000}		
	Line Flux	$1.40^{+0.36}_{-0.32}$		
5. 6.60 keV Line ^c	E_{line}	6.60 ± 0.03	332/307	32.8
	σ	< 0.30		
	EW	24.4 ± 8.0		
	FWHM	< 32000		
	Line Flux	0.67 ± 0.22		
6. 8.00 keV Line ^c	E_{line}	$8.00^{+0.10}_{-0.14}$	322/304	10.0
	σ	< 0.28		
	EW	$45.9^{+33.5}_{-27.7}$		
	FWHM	< 25000		
	Line Flux	$0.78^{+0.57}_{-0.47}$		
7. Fe K β Line ^c	E_{line}	7.06	322/304	0.5
	σ	$< 4.30 \times 10^{-2}$		
	EW	< 29.3		
	FWHM	< 4600		
	Line Flux	< 0.67		
8. Fit Statistics ^d	χ^2/dof	322/304		
	Null Probability	0.36		

Table 1. Spectral Parameters to *Suzaku* XIS in the Fe K band. ^a Γ , photon index; Normalisation in units $\times 10^{-3}$ photons $\text{cm}^{-2} \text{s}^{-1}$; $F_{2.5-10 \text{ keV}}$, absorbed continuum flux from 2.5–10 keV in units $\text{ergs cm}^{-2} \text{s}^{-1}$. ^b Local Galactic absorption (at $z = 0$), units cm^{-2} . ^c E_{line} , line energy in units keV; σ , 1σ line width in units keV; EW, equivalent width in units eV; FWHM, full width at half maximum in units km s^{-1} ; Line Flux in units $\times 10^{-5}$ photons $\text{cm}^{-2} \text{s}^{-1}$. ^d Reduced chi-squared (χ^2/dof) and null hypothesis probability for spectral fit.

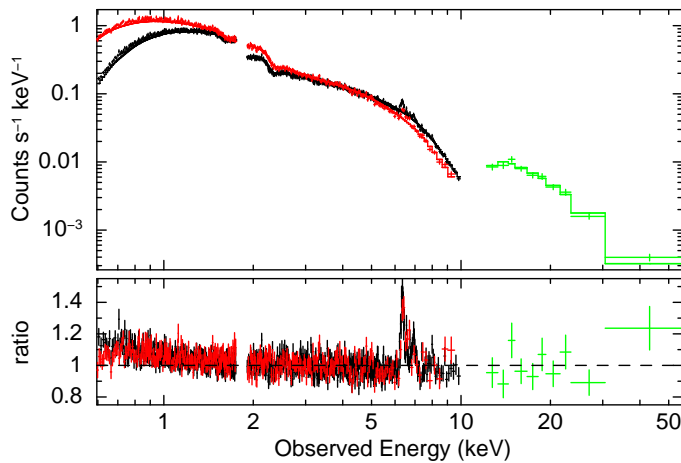


Figure 3. The *Suzaku* spectra of NGC 7213 (in the observed frame) showing the XIS-FI (black), XIS-BI (red) and XIS/PIN (green). An absorbed (Galactic column density) power-law has been fit to the broad-band spectrum. A significant positive residual is observed in the Fe K complex energy range, as well as a weak excess in the < 1 keV energy range.

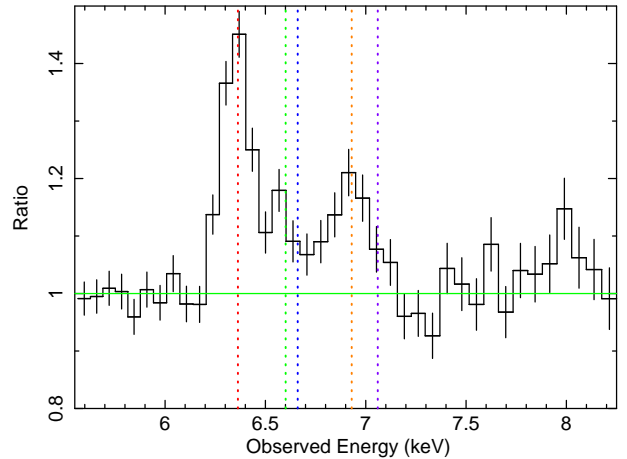


Figure 4. A plot of the ratio of the residuals for XIS-FI of the Fe line complex compared to the power-law continuum. The spectra are binned relative to the half-width at half-maximum of the detector resolution. The vertical dotted lines show the expected line energies of, from left to right, Fe K α , Fe XXV forbidden, Fe XXV $1s-2p$ resonance, Fe XXVI $1s-2p$ Ly α and Fe K β in the observed frame.

few residuals in excess of the power-law continuum indicating little or no reflection component ($R \sim 0.2$, see Section 3.2). Line emission is clearly present with a strong but seemingly relatively narrow Fe $K\alpha$ line at ~ 6.4 keV. As the XIS 1 has a much lower S/N ratio at higher energies above 2 keV, these data were initially excluded from the Fe K line analysis leaving the XIS-FI to be analysed from 2.5–10 keV. The HXD data were also initially excluded as the lack of Compton reflection suggested that the Fe K emission lines could be modelled independently. The HXD and XIS 1 data are re-included in the broad-band fits in Section 3.2.

A simple power-law model of $\Gamma = 1.75 \pm 0.02$ with Galactic absorption evidently resulted in a poor fit ($\chi^2/dof = 739/316$) highlighted by a low null hypothesis probability of 6.67×10^{-36} . A plot of the ratio of the residuals with respect to the power-law continuum from 5.0–8.5 keV (Figure 4) clearly shows X-ray line emission which requires modelling; the most apparent being the Fe $K\alpha$ line from near-neutral material at 6.39 ± 0.01 keV with an intrinsic width of $\sigma < 4.30 \times 10^{-2}$ keV, equivalent width of $EW = 83.1^{+11.0}_{-10.7}$ eV and an observed flux of $F_{K\alpha} = 2.18^{+0.28}_{-0.29} \times 10^{-5}$ photons $\text{cm}^{-2} \text{s}^{-1}$. Adding this line improves the fit significantly with a value of $\Delta\chi^2 = 316.8$ for 3 parameters of interest. However, even upon modelling the strong Fe $K\alpha$ line at 6.39 keV, the fit remains unacceptable (null probability = 3.70×10^{-5}) with further residuals still present between 6.5–7.0 keV indicating K-shell emission from ionised Fe.

Further Gaussian lines were added to fit other prominent emission lines starting with the $1s-2p$ doublet from hydrogen-like iron (Fe XXVI) at 6.95 ± 0.03 keV which corresponds to a value of $\Delta\chi^2 = 57.1$ for an additional 3 parameters of interest. Unlike the 6.39 keV line, this line appears to be resolved compared to the detector resolution with an intrinsic width of $\sigma = 0.10^{+0.05}_{-0.04}$ keV (FWHM $\sim 10\,000$ km s^{-1}), an equivalent width of $EW = 62.3^{+16.0}_{-14.2}$ eV and an observed flux of $F_{\text{line}} = 1.40^{+0.36}_{-0.32} \times 10^{-5}$ photons $\text{cm}^{-2} \text{s}^{-1}$. A third narrow component at a line energy of 6.60 ± 0.03 keV was also modelled, improving the fit by a factor of $\Delta\chi^2 = 32.8$ for a further 3 parameters of interest. A line energy vs. line flux contour plot (Figure 5) shows that this line energy can be rejected at the 99.9% confidence level (for two interesting parameters) as being associated with the resonance line of helium-like iron (Fe XXV) at 6.700 keV ($\Delta\chi^2 \sim 14$) and is just acceptable (rejected at only 90% confidence) as the forbidden line at 6.637 keV (also see Section 3.3.2).² The fact that this indicates that the line at 6.60 keV is more consistent with the forbidden transition of Fe XXV is an interesting discovery since the resonance line is expected to dominate over the forbidden line in a collisionally-ionised plasma (Porquet & Dubau 2000; Bautista & Kallman 2000). Further discussion regarding the origin of this emission can be found in Section 4.2.

A weak, narrow component appeared to remain in the residuals at a line energy of $8.00^{+0.10}_{-0.14}$ keV with an intrinsic width of $\sigma < 0.28$ keV. However the detection is more marginal; adding this extra line component only improved the fit by $\Delta\chi^2 = 10.0$ for 3 parameters. This putative line could possibly be associated with the $1s-3p$ transitions of Fe XXV or Fe XXVI (corresponding

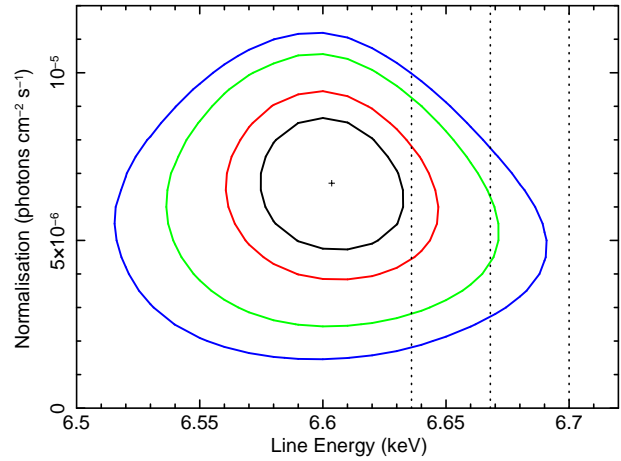


Figure 5. A two dimensional contour plot between line energy and normalisation of the 6.60 keV line at the 68%, 90%, 99% and 99.9% confidence intervals (inner to outer contours respectively) for 2 parameters of interest. The vertical dashed lines show the rest energies of forbidden, intercombination and resonance transitions of the Fe XXV triplet at 6.637, 6.668 and 6.700 keV respectively.

to rest energies of ~ 7.88 and ~ 8.25 keV respectively) or alternatively, it could be due to the $1s-2p$ transition of H-like nickel (corresponding to a rest energy of ~ 8.10 keV). Finally, no neutral $K\beta$ emission was apparent but was still modelled for consistency at a fixed line energy of 7.06 keV, with an intrinsic width, σ , tied to that of the corresponding $K\alpha$ line. The upper limit on the flux of $F_{K\beta} < 0.67 \times 10^{-5}$ photons $\text{cm}^{-2} \text{s}^{-1}$ then provided an upper limit on the $K\beta/K\alpha$ flux ratio of 0.35. A value of $\Delta\chi^2 = 0.5$ revealed that the $K\beta$ line is consistent with the fit to the data but in this instance is not required. Hereafter we include the $K\beta$ line fixed at 13% of the $K\alpha$ flux in all subsequent fits to remain consistent with the theoretical flux ratio for neutral iron (Kaastra & Mewe 1993).

We did also attempt to model the neutral Fe $K\alpha$ emission with a DISKLINE component (Fabian et al. 1989) to test for the presence of any broad, relativistic emission from the inner regions of the accretion disc. We fixed the width of the original Gaussian at 6.39 keV to be narrow ($\sigma = 10$ eV) in order to model emission from distant material and introduced a DISKLINE component to the model with the centroid energy fixed at 6.39 keV and the emissivity index fixed at a standard value of $q = 3$. We also fixed the inner and outer radii of the emission at 6 and 400 R_g from the black hole respectively (where 6 R_g corresponds to the innermost stable orbit for a Schwarzschild black hole) and the inclination angle of the source at $\theta = 30^\circ$. Upon fitting, this returned a value for the flux of the line of $F_{\text{diskline}} < 7.64 \times 10^{-6}$ photons $\text{cm}^{-2} \text{s}^{-1}$ which corresponds to a 90% upper limit on the equivalent width of the line of $EW < 26.8$ eV. This tight constraint appears to exclude the presence of any Fe K emission from the inner accretion disc. We note that no other significant emission or absorption lines are found in the Fe K band. The values of all of the final parameters and fit statistics are noted in Table 1.

3.2 The Broad-Band Spectrum

The first stage of the broad-band spectral analysis was to model the spectra above 10 keV by including the *Suzaku* HXD/PIN data.

² An analysis of the spectrum produced by the XIS Fe-55 calibration source, which produces emission lines from Mn $K\alpha$ and Mn $K\beta$, shows that the absolute XIS energy scale is accurate to within ± 10 eV.

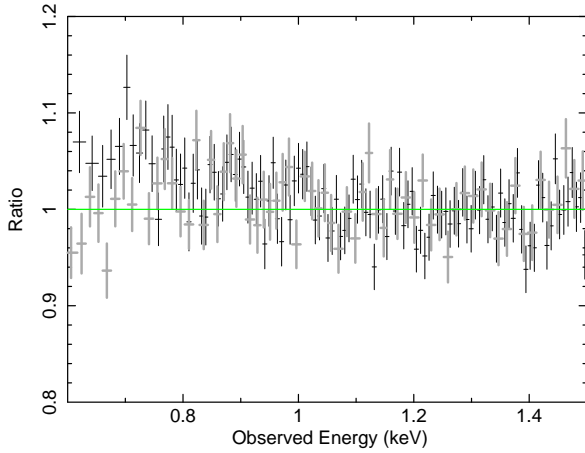


Figure 6. A ratio plot showing the divergence of the XIS 1 detector data (light grey) with that of the XIS 0, 2 and 3 detectors (black) in the soft X-ray regime (see Section 3.2).

To check for consistency, the 22-month time-averaged *Swift* BAT spectra (14–150 keV) were also included (Tueller et al. 2009). This provided an extension of the spectrum far beyond the high energy limit of the HXD PIN. We restricted the energy range of the HXD from 15–50 keV and applied a constant multiplicative factor of 1.16 to account for the cross-normalisation at the XIS nominal pointing position. The constant in front of the BAT data was allowed to be free as the 14–150 keV flux over the 22-month period (2004/12/15–2006/10/27) may have varied (time-averaged flux $F_{14-150} = 5.31 \times 10^{-11} \text{ erg cm}^{-2} \text{ s}^{-1}$). This provided a cross-normalisation factor of 0.75 ± 0.11 for the BAT compared to the *Suzaku* XIS. The power-law component was replaced by an exponential cutoff power-law and we note that no cutoff energy is required in these data. We constrain the 90% lower limit on $E_{\text{cut}} > 350 \text{ keV}$. A simultaneous *XMM-Newton* and *BeppoSAX* PDS observation published by Bianchi et al. (2004) required a high energy cutoff with a value of $E_{\text{cut}} = 90^{+50}_{-20} \text{ keV}$. However, fixing the cutoff energy at 90 keV in our *Suzaku*+BAT spectrum results in a worse fit with $\Delta\chi^2 = 35$ supportive of the notion that the cutoff appears to be at significantly higher energy in these data.

The residuals in the hard X-ray regime show very little excess flux above 10 keV when modelled with a power-law indicating a lack of a Compton reflection component. To test for this, we included the PEXRAV model (Magdziarz & Zdziarski 1995) which is an additive component incorporating the reflected continuum from a neutral slab. We tied the photon index of the power-law incident upon the reflector to that of the power-law continuum and fixed the elemental abundances to Solar (Anders & Grevesse 1989). We also fixed the cosine of the inclination angle of the source to 0.87 and tied the folding energy to the cutoff energy of the power-law at $\sim 1000 \text{ keV}$, consistent with no cut-off as above. The inclusion of the PEXRAV component resulted in a reflection scaling factor value of $R = 0.18^{+0.23}_{-0.14}$, consistent with the *XMM-Newton*/*BeppoSAX* analysis of Bianchi et al. (2004) who find $R < 0.19$. The inclusion of this component corresponds to $\Delta\chi^2 \approx 5.0$ suggesting that this component is only marginally required. This resulted in a fit statistic $\chi^2/\text{d.o.f.} = 486/446$, acceptable with a null hypothesis probability of 0.10.

The next step was to model the entire broad-band spectra by including the XIS data below 2.5 keV. As the signal-to-noise ratio decreases at lower energies, the spectra were only included down to 0.6 keV for each XIS. The data were also ignored from 1.7–1.9 keV so as not to include the silicon absorption edge due to the detectors. The inclusion of these data resulted in a slightly worse fit with a null probability of 2.98×10^{-3} . Residuals were observed at energies $< 2 \text{ keV}$ hinting at the presence of a weak soft excess (e.g., Figure 3). Upon closer inspection of these residuals it was noted that the XIS 1 (BI) detector data slightly diverged with that of the remaining XIS detectors (Figure 6), even when the photon index of the power-law continuum was allowed to vary between detectors. As the XIS 0, 2 and 3 (FI) were all self-consistent, this divergence was possibly caused by calibration effects around the oxygen K detector edge. To account for this, the data from the XIS 1 detector were ignored below 0.7 keV.

In an attempt to then model the observed soft excess, we added a MEKAL thermal plasma component incorporating the emission spectra from a hot diffuse gas (Starling et al. 2005). It is worth noting that a featureless blackbody component models the soft excess with an equally good fit as there are no strong lines. However, this model was not considered any further as the lack of evidence for a strong Big Blue Bump (Wu et al. 1983) suggested little thermal emission directly from the disc (Starling et al. 2005). The addition of the MEKAL component gave a best-fitting thermal plasma temperature of $k_B T = 0.27^{+0.05}_{-0.04} \text{ keV}$ and resulted in an overall better fit with $\chi^2/\text{d.o.f.} = 1104/1022$ compared to 1151/1024 before the MEKAL component was added³. The luminosity of the MEKAL component was calculated at $L = 2.14 \times 10^{40} \text{ erg s}^{-1}$ corresponding to only 1% of the the total luminosity in the 0.5–10 keV band. As no further significant residuals were observed in the spectra (Figure 7), this became our accepted broad-band model, the final parameters of which are summarised in Table 2 (note that the full broad-band model from 0.6–150 keV also resulted in a tighter constraint on the reflection scaling factor, R , the best-fit value of which is shown in Table 2). A plot of the relative unfolded model contributions is shown in Figure 8.

3.3 Comparison with Past Observations

3.3.1 *XMM-Newton* & *BeppoSAX*

We tested for any long-term variations in the source by applying our best-fit broad-band *Suzaku* model to the 2001 simultaneous *XMM-Newton* (30 ks exposure) and *BeppoSAX* PDS (38 ks exposure) observation (May 2001; see Table 3), as published previously by Bianchi et al. (2003, 2004) and Starling et al. (2005). The ratio of the *XMM-Newton* EPIC-pn spectrum from 0.3–10 keV to the best fit *Suzaku* model, with continuum parameters described in Table 2, is shown in Figure 9. It can be seen that compared to the *Suzaku* XIS spectrum, the pn spectrum is steeper, while overall the flux was slightly lower in the *XMM-Newton* data with a value of $2.19 \times 10^{-11} \text{ erg cm}^{-2} \text{ s}^{-1}$ over the 2–10 keV energy range. We also note that the flux obtained from the *BeppoSAX* data was lower than that obtained with the *Suzaku* HXD over the 12–100 keV

³ Modelling the soft excess with an APEC component was also considered (<http://hea-www.harvard.edu/APEC/>; Smith et al. 2001) although at the *Suzaku* resolution here, the fit was identical to that obtained with the MEKAL thermal plasma.

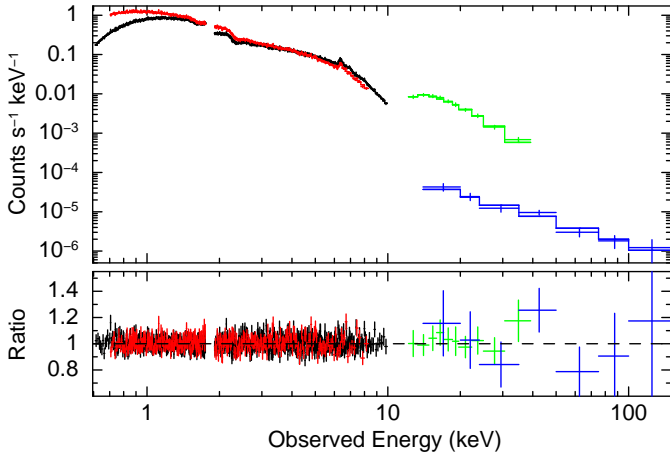


Figure 7. The broad-band spectra of NGC 7213 (in the observed frame) with the inclusion of the *Swift* BAT spectra (blue). A plot of the ratio of the residuals to the model described in Section 3.2 and Table 2 is shown in the lower panel. No significant residuals are present.

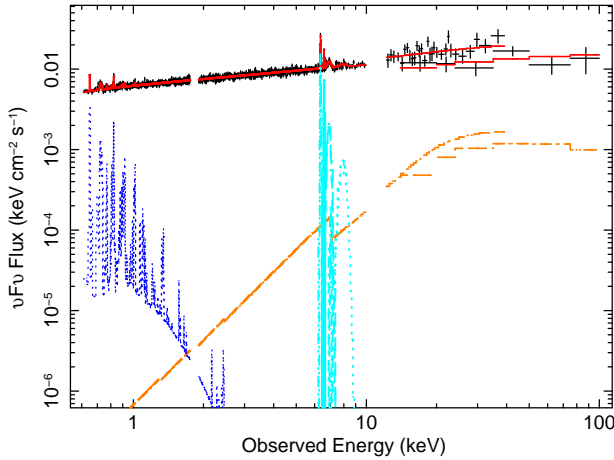


Figure 8. A plot showing the relative contributions of the individual model components across the broad-band 0.6–100 keV *Suzaku*+BAT energy range (see Section 3.2 for details). The PEXRAV neutral reflection component is shown in orange over the 1–100 keV energy range whilst the soft collisionally-ionised MEKAL component (at energies <3 keV) is shown in navy blue. The emission in the Fe K complex is modelled with individual Gaussians. The red curve spanning the whole energy range shows the sum of all the model components (including the absorbed power-law continuum) superimposed on the data.

range (2.46×10^{-11} compared to 3.81×10^{-11} erg cm $^{-2}$ s $^{-1}$ respectively). Since the photon index of the power-law continuum is quite hard in this source, this difference could simply arise from small changes in the intrinsic power-law. The model is generally in good agreement with the data although subtle changes in the continuum can be observed, with the spectral curvature being more apparent in the *XMM-Newton* data, e.g., with the spectrum being noticeably steeper below 2 keV, but somewhat flatter above 3 keV. No strong residuals are present in the iron K band, which suggests that the iron line emission has remained constant between the 2001 *XMM-Newton* and 2006 *Suzaku* observations.

Model Component	Fit Parameter	Value
1. Cutoff Power-law ^a	Γ	1.74 ± 0.01
	High Energy Cutoff	> 350
	Normalisation	$6.28^{+0.05}_{-0.03}$
2. Galactic Absorption ^b	N_H	1.10×10^{20}
3. PEXRAV ^c	$ R $	$0.09^{+0.19}_{-0.08}$
4. MEKAL ^d	$k_B T$	$0.27^{+0.05}_{-0.04}$
	Normalisation	$1.27^{+0.59}_{-0.38}$
	Luminosity	2.14×10^{40}
5. Fit Statistics ^e	χ^2/dof	1100/1041
	Null Probability	4.40×10^{-2}

Table 2. Spectral Parameters of continuum fit in the 0.6–150 keV range (see Section 3.2 for details). ^a Γ , photon index; High energy cutoff in units keV; Normalisation in units $\times 10^{-3}$ photons cm $^{-2}$ s $^{-1}$. ^b Local Galactic absorption (at $z = 0$), units cm $^{-2}$. ^c $|R|$, reflection scaling factor, where a value $R = 1$ corresponds to reflection from neutral material subtending 2π sr. ^d $k_B T$, plasma temperature in units keV; Normalisation (Emission Measure = $\int n_e n_H dV$) in units $\times 10^{63}$ cm $^{-3}$. ^e Reduced chi-squared (χ^2/dof) and null hypothesis probability for spectral fit.

To quantify the changes in the spectrum, the single power-law continuum used to fit the *Suzaku* data in Sections 3.1 and 3.2 was replaced with a broken power-law, breaking at $2.19^{+0.34}_{-0.30}$ keV with Γ values of 1.84 ± 0.01 and 1.71 ± 0.02 below and above this energy break respectively. Furthermore, a slight softening of the spectrum below 1 keV in the *XMM-Newton* data, as suggested by the bump in the residuals around 0.9 keV (which may due to the Ne IX triplet or a blend of emission from iron L-shell lines), indicates that the single temperature MEKAL component obtained from the *Suzaku* data was not sufficient to model the soft excess. Thus a second MEKAL component was added to the model with a higher temperature of $k_B T = 0.86^{+0.20}_{-0.14}$ keV, which significantly improved the fit ($\Delta\chi^2 = 19.2$) compared to the model with only a single temperature plasma. The fit parameters of this best-fit model to the *XMM-Newton* data are summarised in Table 4.

For consistency this two temperature MEKAL model was then applied to the 2006 *Suzaku* dataset. The temperatures and normalisations of the MEKAL were kept fixed at the best-fit values from the *XMM-Newton* data, as an extended diffuse collisional plasma may not be expected to vary significantly over time (note that if the parameters are allowed to vary, the values obtained from *Suzaku* are consistent with the *XMM-Newton* data, within the errors). The broken-powerlaw continuum parameterisation was also retained from the *XMM-Newton* fit, although the photon indices and normalisations were allowed to vary. A comparison of fit parameters for the *Suzaku* and *XMM-Newton* observations is shown in Table 4. No other significant variations were observed between the two observations; the Fe K line parameters appear to be consistent with constant values (within the errors) for the centroid energy and line fluxes, while the 2001 *BeppoSAX* PDS data show no evidence for a reflection hump above 10 keV (with $R < 0.2$; see also Bianchi et al. 2004), consistent with what is found by the *Suzaku* HXD. Furthermore, the lower limit on the high energy cutoff value is also constrained to >300 keV (see also Dadina 2008), in good agreement with the HXD and *Swift* BAT.

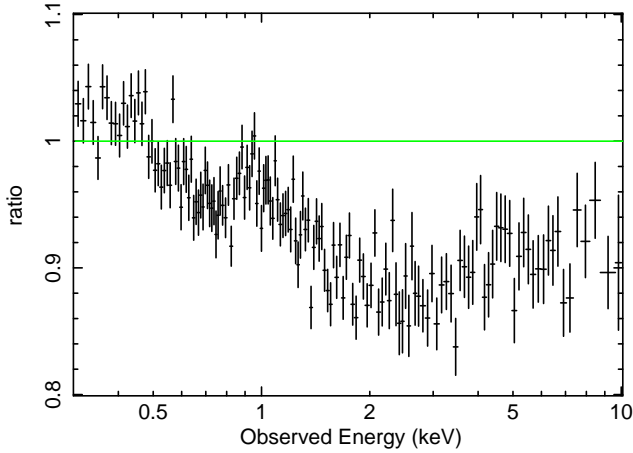


Figure 9. Data/Model residuals of the 2001 *XMM-Newton* EPIC-pn data to the *Suzaku* model listed in Table 2. The *XMM-Newton* data show the source to have a slightly steeper spectrum compared to *Suzaku* at energies below 2 keV, while overall the continuum flux in the 2–10 keV band is lower in the *XMM-Newton* data in 2001 compared to *Suzaku* in 2006. See Section 3.3 for details.

Date	Mission	Instrument	Exposure (ks)
27/05/2001	<i>BeppoSAX</i>	MECS	61
		PDS	38
29/05/2001	<i>XMM-Newton</i>	EPIC-PN	30
15/12/2004 - 27/10/2006	<i>Swift</i>	BAT	2300
22/10/2006	<i>Suzaku</i>	XIS/HXD	90
06/08/2007	<i>Chandra</i>	HETG	148

Table 3. Log of observations of NGC 7213. See Section 3.3 for details.

3.3.2 *Chandra* HETG

The emission line at 6.60 keV in the *Suzaku* XIS spectrum is found to be rejected at the $> 99.9\%$ confidence level as arising from the resonance transition of helium-like iron (see Section 3.1 and Figure 5). As a consistency check, we modelled the archival *Chandra* HETG spectrum (using the latest version of the calibration database; v4.2.2) at Fe K with an absorbed power-law and parameterised the emission lines with simple Gaussians consistent with the values found by Bianchi et al. (2008) (also see Table 4) with emission lines at 6.40, 6.72 and 6.99 keV. Fixing an additional narrow line ($\sigma = 10$ eV) at 6.60 keV (as required by *Suzaku*) in the HETG spectrum was not required by the data but resulted in a value for the equivalent width of $EW < 21.2$ eV, which is consistent with the equivalent width of $EW = 24.4 \pm 8.0$ eV found in the *Suzaku* XIS. Likewise, including a narrow Gaussian in the *Suzaku* spectrum with the centroid energy fixed at 6.72 keV (as found by *Chandra*) is also not required by the XIS data but yields an upper limit on the equivalent width of $EW < 14.3$ eV, again consistent with the equivalent width of $EW = 24.0 \pm 17.0$ eV found by Bianchi et al. (2008) with the *Chandra* HETG. Therefore, it appears that the Fe K parameters in both datasets are consistent with each other with no evidence of variability detected within the errors.

4 DISCUSSION

In this section the possible origin of both the neutral and ionised iron K line emission from NGC 7213 is discussed along with its implications for the nature of the central engine in this source.

4.1 The Origin of the Neutral Fe K α Line

We first investigated the possibility of whether a distant Compton-thick reflector, e.g., such as the pc-scale torus, could account for the neutral Fe K α emission. The tight constraint on the reflection fraction of $R = 0.09^{+0.19}_{-0.08}$, obtained in Section 3.2 (also see Table 2), appears to rule out the possibility of the 6.39 keV line originating via scattering off Compton-thick matter since, for an Fe K α line with an equivalent width of ~ 80 eV (as observed here), a strong reflection scaling factor value of $R \approx 0.6$ would be required (George & Fabian 1991). To test this further, the ionised reflection model REFLIONX (Ross & Fabian 2005) was used in place of the simple 6.39 keV Gaussian emission and PEXRAV model for the Compton-scattered continuum off neutral material. The other model components, as described in Section 3.2 (also see Tables 1 and 2), were adopted and are identical in the spectral fits. The REFLIONX model consists of the emergent spectrum for a photo-ionised optically-thick slab of gas when irradiated by a power-law spectrum, with a high energy exponential cut-off of 300 keV, using the abundances of Anders & Ebihara (1982). The advantage of the REFLIONX model is that it self-consistently computes both the reflected continuum and line emission for the astrophysically abundant elements.

We initially fixed the iron abundance to Solar, while the redshift of the reflector was found to be consistent with the cosmological redshift of the source, with no net (e.g., gravitational) redshift. Given the narrow unresolved iron K α emission observed in the *Suzaku* spectrum, no additional velocity broadening was applied to the reflected spectrum. We also fixed the reflector ionisation parameter⁴ at a value of $\xi = 10$ erg cm s $^{-1}$ (the lowest value allowed by the model), corresponding to near-neutral iron (i.e., iron atoms typically in a low ionisation state corresponding to Fe I–XVII). This model provides an upper limit on the reflection scaling factor of $R < 0.16$, consistent with what was found by the PEXRAV model in Section 3, but results in a relatively poor fit to the *Suzaku*+BAT data of $\chi^2/d.o.f. = 810/715$ (null probability = 7.22×10^{-3}). This is due to the fact that the model underpredicts the amount of iron K α emission, leaving a significant positive residual at ~ 6.4 keV in the *Suzaku* XIS data. Allowing the Fe abundance to vary to enhance the iron K emission results in an acceptable fit of $\chi^2/d.o.f. = 745/714$ corresponding to a null hypothesis probability of 0.21 (with $R < 0.06$). However, in order to adequately model the iron K α line, this requires an overabundance of Fe by a factor of ~ 10 with respect to Solar (the 90% confidence lower limit on this value is still 4 times Solar).

It therefore appears that the lack of an observed Compton reflection hump in the data above 10 keV means that the reflection and Fe K α emission cannot be simultaneously modelled in this

⁴ Note that in the REFLIONX ionised reflection model the ionisation parameter is defined as $\xi = \frac{4\pi F}{n}$ and has units erg cm s $^{-1}$, where F is the illuminating flux incident upon the reflector (integrated over the energy range 100 eV to 1 MeV) and n is the gas density in cm $^{-3}$.

Model Component	Fit Parameter	<i>Suzaku</i>	<i>XMM-Newton</i> & <i>BeppoSAX</i>	<i>Chandra</i> /HETG
Flux ^a	$F_{0.5-2}$	1.37	1.29	-
	F_{2-10}	2.44	2.19	-
	F_{12-100}	3.81	2.46	-
Broken Powerlaw ^b	Γ_1	$1.94^{+0.09}_{-0.06}$	1.84 ± 0.01	-
	E_{break}	$0.93^{+0.06}_{-0.07}$	$2.19^{+0.34}_{-0.30}$	-
	Γ_2	1.74 ± 0.01	1.71 ± 0.02	-
	Normalisation	$6.11^{+0.09}_{-0.16}$	$5.92^{+0.03}_{-0.04}$	-
MEKAL ^c	$k_B T_1$	FIXED	$0.24^{+0.07}_{-0.06}$	-
	Norm ₁	FIXED	$6.60^{+4.06}_{-3.81}$	-
	$k_B T_2$	FIXED	$0.86^{+0.20}_{-0.14}$	-
	Norm ₂	FIXED	$7.63^{+2.74}_{-2.65}$	-
	L_{total}	1.99	1.99	-
Fe K α Line ^d	$E_{K\alpha}$	6.39 ± 0.01	6.40 ± 0.02	6.40 ± 0.01
	EW _{Kα}	$83.1^{+11.0}_{-10.7}$	$85.9^{+14.0}_{-14.4}$	120^{+40}_{-30}
	Line Flux _{Kα}	$2.18^{+0.28}_{-0.29}$	$2.33^{+0.38}_{-0.39}$	$2.9^{+0.9}_{-0.7}$
6.60 keV Line ^d	$E_{6.60}$	6.60 ± 0.03	$6.66^{+0.04}_{-0.05}$	$6.72^{+0.01}_{-0.02}$
	EW _{6.60}	24.1 ± 7.9	27.4 ± 11.6	24 ± 17
	Line Flux _{6.60}	0.67 ± 0.22	0.78 ± 0.33	0.7 ± 0.5
6.95 keV Line ^d	$E_{6.95}$	6.95 ± 0.03	6.91 ± 0.08	$6.99^{+0.02}_{-0.01}$
	EW _{6.95}	$62.3^{+16.0}_{-14.2}$	37.1 ± 18.8	60 ± 30
	Line Flux _{6.95}	$1.40^{+0.36}_{-0.32}$	0.89 ± 0.45	1.3 ± 0.6
Statistics	$\chi^2/d.o.f.$	747/723	846/872	-
	Null Probability	0.26	0.73	-

Table 4. Spectral parameters of the broad-band fit in the 0.6–150 keV energy range for the 2006 *Suzaku* and 2001 simultaneous *XMM-Newton* and *BeppoSAX* observations (see Section 3.3 for details). The Fe-line complex parameters from the 2007 *Chandra*/HETG observation (reported by Bianchi et al. 2008) are also shown for ease of comparison. ^a Continuum flux in the specified range in units $\times 10^{-11}$ erg cm $^{-2}$ s $^{-1}$. ^b Γ , photon index; E_{break} in units keV; Normalisation in units $\times 10^{-3}$ photons cm $^{-2}$ s $^{-1}$. ^c $k_B T$, plasma temperature in units keV; Normalisation ($= \int n_e n_H dV$) in units $\times 10^{62}$ cm $^{-3}$; Total MEKAL luminosity from 0.5–10 keV in units 10^{40} erg s $^{-1}$. All MEKAL fit parameters in the *Suzaku* dataset are fixed at the best-fit values from the XMM data. ^d E_{line} , line energy in units keV; EW, equivalent width in units eV; Line Flux in units $\times 10^{-5}$ photons cm $^{-2}$ s $^{-1}$.

way, seemingly ruling out a reflection origin for the Fe K α emission, as also suggested by Bianchi et al. (2003) on the basis of the *BeppoSAX* data. Indeed, an acceptable fit can only be obtained if the abundances are assumed to be greatly super-Solar, at odds with the modest spread of values found by Perola et al. (2002) from a sample of nine bright Type 1 Seyferts and NELGs (Narrow Emission-Line Galaxies) observed with *BeppoSAX*. Thus it appears unlikely that the 6.39 keV emission originates via reflection off Compton-thick matter unless the material covers a very small solid angle (< 1 sr) and is extremely iron over-abundant.

Instead it is perhaps more likely that the near-neutral iron K α line originates in Compton-thin matter, covering a higher fraction of 4π steradians solid angle. Indeed, an estimate of the column density of the K α -emitting material can be made using the calculations of Yaqoob et al. (2010) where an analytic expression relating the efficiency of the Fe K α line production and the column density of the emitting material is derived in the optically-thin limit. The production efficiency of the Fe K α line is calculated by:

$$\chi_{\text{Fe K}\alpha} = \frac{I_{\text{Fe K}\alpha, n}}{\int_{E_K}^{\infty} E^{-\Gamma} dE}. \quad (1)$$

Here, E_K is the threshold energy for Fe K-shell absorption and $I_{\text{Fe K}\alpha, n}$ refers to the line flux renormalised to an incident continuum with a flux of 1 photon cm $^{-2}$ s $^{-1}$ keV $^{-1}$ at 1 keV. Γ is the photon index assuming an incident power-law continuum. Adopting the Verner et al. (1996) value for E_K of 7.124 keV, we calculate an Fe K α line production efficiency of $\sim 1\%$ for NGC

7213. In the Compton-thin case, we find that this results in an estimate on the column density of the K α -emitting material of $N_H \sim 2 \times 10^{23}$ cm $^{-2}$ using the analytic expression derived by Yaqoob et al. (2010) (equation 4 in the aforementioned publication). Although this value is consistent with that found by Bianchi et al. (2008), the expression is valid only in the Compton-thin limit which begins to break down for $N_H > 2 \times 10^{22}$ cm $^{-2}$ as the optical depth of the Fe K line photons to absorption and scattering becomes non-negligible (see Yaqoob et al. 2010, Figure 2). However, accounting for these effects, according to the calculations of Yaqoob et al. (2010) and Murphy & Yaqoob (2009), a column density of $N_H \sim 3 - 4 \times 10^{23}$ cm $^{-2}$ can result in an Fe K α line efficiency of 1% for a face-on geometry covering 2π sr in their toroidal X-ray reprocessor model. Thus the Fe K α line may originate in a Compton-thin torus or perhaps the outer BLR clouds, as suggested by Bianchi et al. (2005), although the covering fraction would perhaps be slightly high in the latter case (Netzer & Laor 1993).

4.2 The Origin of the Highly Ionised Fe

We investigated the possibility of an ionised accretion disc as a potential origin for the 6.60 and 6.95 keV emission lines. To test this scenario, we attempted to model the two ionised emission lines by a REFLIONX component with a high ionisation parameter of $\log \xi = 3.0^{+0.2}_{-0.1}$ erg cm s $^{-1}$. The remainder of the *Suzaku* spectrum was modelled as before, i.e., a cut-off power-law for the continuum emission, a single temperature thermal MEKAL component for the weak soft X-ray excess and a narrow Gaussian centered at 6.39 keV for the neutral iron K α emission. No relativistic blurring

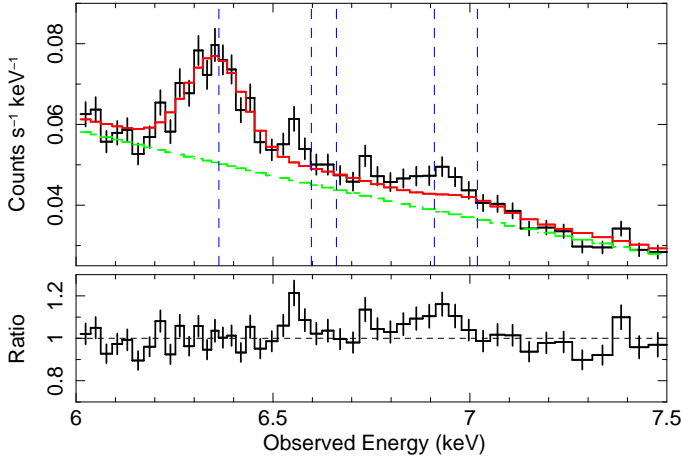


Figure 10. A plot showing the inability to model the highly ionised Fe emission at 6.60 keV and 6.95 keV with an ionised reflector therefore suggesting a non-reflection origin for these lines (as described in Section 4.2). The continuum level is shown in green and the lower panel shows the ratio of the residuals to the model. The neutral $\text{Fe K}\alpha$ line at 6.39 keV is modelled with a Gaussian. The vertical dotted lines show the expected line energies of, from left to right, $\text{Fe K}\alpha$, Fe XXV forbidden, $\text{Fe XXV } 1s-2p$ resonance, $\text{Fe XXVI } 1s-2p$ and $\text{Fe K}\beta$ in the observed frame.

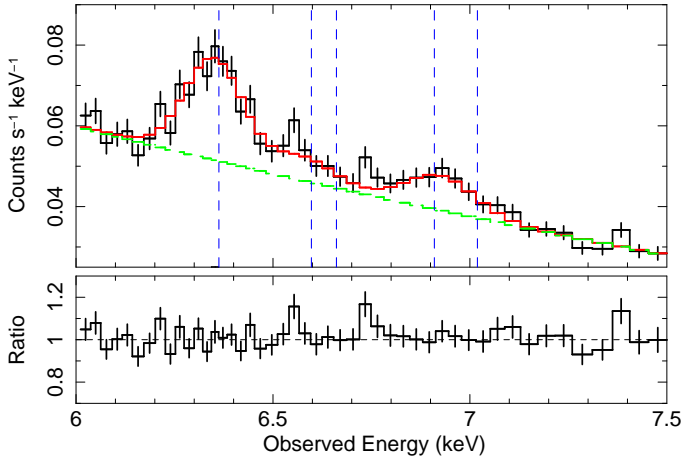


Figure 11. A plot showing the fit obtained when the highly ionised Fe is modelled with a photo-ionised XSTAR grid with $\sigma = 3000 \text{ km s}^{-1}$ and $\log \xi = 4.4 \text{ erg cm s}^{-1}$ (as described in Section 4.2.2). The continuum level is shown in green and the lower panel shows the ratio of the residuals to the model. The neutral $\text{Fe K}\alpha$ line at 6.39 keV is modelled with a Gaussian. The vertical dotted lines show the expected line energies of, from left to right, $\text{Fe K}\alpha$, Fe XXV forbidden, $\text{Fe XXV } 1s-2p$ resonance, $\text{Fe XXVI } 1s-2p$ and $\text{Fe K}\beta$ in the observed frame.

was applied. This resulted in a poor fit of $\chi^2/d.o.f. = 791/717$ (null probability = 2.79×10^{-2}) with the model unable to account for the ionised emission from either Fe XXV or Fe XXVI (see Figure 10). Indeed due to the large intrinsic electron scattering depth at such high values of ξ , the lines in the reflection model become too broadened and so are unable to model the relatively narrow 6.60 and 6.95 keV lines that are observed in the *Suzaku* spectrum. Furthermore the 90% confidence upper-limit on the reflection frac-

tion for the highly ionised reflector is restricted to $R < 0.06$, which seemingly allows us to reject the presence of a highly ionised Compton-thick medium in NGC 7213, such as a highly ionised, but Compton-thick inner accretion disc.

In addition, the inability to model the neutral $\text{Fe K}\alpha$ emission with a low ionisation reflector (see Section 4.1) coupled with the apparent lack of a Compton hump $> 10 \text{ keV}$ means that this source exhibits no evidence at all for any Compton-thick material, either neutral or ionised. Furthermore, the data do not appear to show any relativistic signatures since the neutral and ionised iron lines appear to be narrow (or only moderately broad in the case of Fe XXVI), thus ruling out any emission from the innermost regions around the black hole. Combining the lack of evidence for any Compton-thick matter in this source with the lack of any relativistic signature seems to suggest the complete absence of an inner optically-thick accretion disc in NGC 7213. Instead it may support the notion of an accretion disc which is truncated at some radius with the inner regions replaced by some form of Radiatively Inefficient Accretion Flow (RIAF; Narayan & Yi 1995), where the low efficiency of the inner, hot corona leads to much of the energy being advected into the black hole rather than radiated away.

4.2.1 Collisionally-Ionised Model

We instead investigated the possibility of a collisionally-ionised origin for the highly ionised Fe K emission which we modelled with a high temperature broadened APEC component (Smith et al. 2001). This required a temperature of $k_B T = 13.03^{+2.61}_{-2.86} \text{ keV}$ and velocity broadening, $\sigma \sim 2500 \text{ km s}^{-1}$, resulting in a fit statistic of $\chi^2/d.o.f. = 788/716$. Inspection of the data around the iron K band reveals that the collisionally-ionised model over-predicts the contribution of the resonance line compared to the forbidden line of Fe XXV , which leaves some excess line flux near 6.60 keV unmodelled, although the Fe XXVI line is modelled well. Thus, although the collisional model cannot be ruled out with high confidence in the present data, given that the energy of the 6.60 keV line appears more consistent with the forbidden rather than resonance transition of Fe XXV , an additional photo-ionised component would perhaps be required to model this line (see Section 4.2.2).

An estimate on the density of the collisionally-ionised material can be calculated from the normalisation of the APEC code, which returns $\int n^2 dV \sim 10^{64} \text{ cm}^{-3}$. If the observed broadening of the line is assumed to be due to a Keplerian orbit ($\sigma \sim 0.1 \text{ keV}$ corresponding to a few 10^4 km s^{-1} ; see Table 1), we can calculate an estimate on the radius of the emitting material from the central black hole of a few $10^4 R_g$, where $1 R_g = 1.5 \times 10^{13} \text{ cm}$ for a black hole mass of $10^8 M_\odot$ (Nelson & Whittle 1995). Adopting this radius of $R \sim 1.5 \times 10^{17} \text{ cm}$ results in an estimate of $n \sim 10^6 \text{ cm}^{-3}$ for the density of the emitting material.

If the collisional gas is indeed responsible for some of the highly ionised Fe emission then we note that the conditions of the gas must be different from those in the lower temperature gas used to model the weak soft excess at energies $< 1 \text{ keV}$ (see Section 3.2). The two components require very different temperatures ($0.27^{+0.05}_{-0.04}$ and $13.03^{+2.61}_{-2.86} \text{ keV}$ for the low and high temperature gases respectively) and we note that any contribution from one distinct zone of emission to the other is negligible (i.e., no significant emission from the lower temperature zone is found to be contributing the emission at Fe K and vice-versa). However, the two zones

of gas could be linked by their origin albeit on completely different scales with the emission from the lower temperature gas originating at a much greater distance from the black hole.

4.2.2 A Photo-ionisation Model for the Ionised Iron K Emission

An alternative origin for the lines could be emission from a photo-ionised, but Compton-thin plasma. We modelled this scenario using the XSTAR 2.1ln11 code (Kallman & McCray 1982), which incorporates the abundances of Grevesse, Noels & Sauval (1996). We initially modelled the lines using a single zone of emission with Solar abundances and a turbulent velocity width of 200 km s^{-1} . The best-fit value of the ionisation parameter was $\log \xi = 3.7 \pm 0.3$ (where the ionisation parameter in XSTAR is defined as in equation 3), which resulted in an acceptable fit with $\chi^2/d.o.f. = 779/715$ (null probability = 4.73×10^{-2}). Even so, some slight excess residuals were apparent, particularly around the 6.95 keV line, which might suggest there is some intrinsic velocity broadening of the ionised lines. For instance, as measured from Section 3.1, the H-like line appears to have a FWHM of $\sim 10\,000 \text{ km s}^{-1}$.

Thus an alternative XSTAR grid was used with a higher turbulence velocity of $\sigma = 3000 \text{ km s}^{-1}$. This resulted in a slightly better fit of $\chi^2/d.o.f. = 765/715$ (null probability = 8.50×10^{-2}), with an ionisation parameter of $\log \xi = 4.4 \pm 0.1$ (see Section 4.3.3 for a calculation of the lower limit on the column density). This fit is significantly better than the one obtained with the collisionally-ionised model (Section 4.2.1) with $\Delta\chi^2 = 23$ between the two models. A plot of this model superimposed on the data is shown in Figure 11. We also calculated the 90% uncertainty on the redshift of the zone allowing us to constrain the net velocity shift of the ionised emitter to be $v = +650_{-1500}^{+1650} \text{ km s}^{-1}$, where a positive velocity denotes redshifted / infalling material. Thus the data do not formally require a velocity shift in this model. Further zones of ionised matter are also not required by the data.

Both high and low turbulence models appear to give good fits over the iron K band, with the 6.95 keV emission line originating from the Fe XXVI Ly α doublet and the 6.60 keV He-like line arising due to a blend of the forbidden and intercombination lines at 6.637 and 6.668 keV respectively. In the low density limit assumed in the XSTAR model here (where $n < 10^{16} \text{ cm}^{-3}$), the He-like emission is from an approximately equal mixture of the forbidden and intercombination lines, with a negligible contribution from the resonance line at 6.700 keV. Note that some weak emission via satellite lines of lower ionisation iron (i.e., Fe XXIII-XXIV) could also be contributing to this blend of emission although at the high ionisation parameter inferred here (of $\log \xi \sim 4$), this contribution is likely to be negligible (Kallman & McCray 1982). However, future calorimeter-based spectroscopy, e.g., with Astro-H, will be required to spectrally resolve all the line emission components associated with the He-like triplet of iron and to constrain the intrinsic velocity broadening.

We also note that if the highly ionised iron lines are originating in photo-ionised gas then the possibility remains that a similar photo-ionised gas but with a much lower ionisation parameter could be responsible for the weak soft X-ray lines observed at energies $< 1 \text{ keV}$. However, Starling et al. (2005) analysed the results of an XMM-Newton RGS observation of NGC 7213 and found that a collisionally-ionised thermal plasma was preferred by the data from

consideration of the 'G' ratio (Porquet & Dubau 2000) of the O VII triplet.

4.2.3 The Location of the Highly Ionised Gas

From consideration of various photo-ionised and collisionally-ionised models, it appears that the 6.60 and 6.95 keV lines are consistent with originating in a photo-ionised medium, although the H-like Ly α line appears to be quite strong with an equivalent width of $\sim 60 \text{ eV}$. Bianchi & Matt (2002) calculate the equivalent widths of Fe XXV and Fe XXVI lines with respect to both the reflected and total continua and show that an equivalent width of $\sim 15 \text{ eV}$ for H-like Fe would be expected if it originated in material of column density, $N_{\text{H}} \sim 10^{23} \text{ cm}^{-2}$, with an ionisation parameter of $\log \xi \sim 3.5$, photon index of $\Gamma = 1.7$ and a covering fraction, $f = 1$. To test whether our equivalent width of $\sim 60 \text{ eV}$ was feasible we calculated a lower limit on the column density of the photo-ionised material in the case of one single zone of emission.

For a uniform, spherical, Compton-thin shell, the normalisation of the photo-ionised emission component is defined within the XSTAR code by⁵:

$$k = f_{\text{cov}} \frac{L_{\text{ion}}}{D^2} \quad (2)$$

where f_{cov} is the covering fraction of the material (i.e., $f_{\text{cov}} = 1$ for matter covering $4\pi \text{ sr}^{-1}$), L_{ion} is the ionising luminosity in units $10^{38} \text{ erg s}^{-1}$ from 1 to 1000 Rydbergs and D is the distance to the source in kpc. Physically the XSTAR normalisation is simply proportional to the observed X-ray flux of the source multiplied by the covering fraction of the photo-ionised gas. Thus the appropriate value of this normalisation, k , for NGC 7213 can be calculated assuming a covering fraction of 1. For the luminosity and distance of NGC 7213, this results in a value of $k = 9.0 \times 10^{-5}$ in units $10^{38} \text{ erg s}^{-1} \text{ kpc}^{-2}$, where we have adopted a distance of 25 000 kpc to NGC 7213 (Mould et al. 2000). The value used for the ionising luminosity was derived from an extrapolation of the broken power-law continuum in Table 4, integrated from 1 to 1000 Rydbergs and is found to be $5.61 \times 10^{42} \text{ erg s}^{-1}$, comparable to the estimate of the bolometric luminosity of $\sim 9 \times 10^{42} \text{ erg s}^{-1}$ by Starling et al. (2005).

In the model used in Section 4.2.2, we have fixed the normalisation of the additive XSTAR emission component to the above value and thus assumed a fully covering shell of gas around NGC 7213, with the appropriate source luminosity and distance from above. The column density was then allowed to vary within the XSTAR model, in order to fit the ionised iron K emission lines. This provided a best fit value for the column density of $N_{\text{H}} = 4.0_{-0.8}^{+0.5} \times 10^{23} \text{ cm}^{-2}$. The 90% confidence lower limit on the column density is $N_{\text{H}} > 3.2 \times 10^{23} \text{ cm}^{-2}$ for a fully covering spherical shell of gas, with an ionisation parameter of $\log \xi \sim 4$ as above. For a shell that does not fully cover the source, then the column density will need to be higher to compensate for the lower covering. This is in good agreement with the calculations of Bianchi & Matt (2002), who predict an equivalent width for Fe XXVI Ly α of 15 eV for a column density of 10^{23} cm^{-2} , compared to the observed 60 eV equivalent width in the case of NGC 7213, but for a

⁵ see

<http://heasarc.gsfc.nasa.gov/docs/software/xstar/docs/html/node94.html>

column density approximately 3–4 times higher.

In order to better constrain the origin of the Fe XXVI Ly α line it is important to estimate a value for the distance of the emitting material. Assuming a uniformly ionised, spherical shell of gas, the ionisation parameter in XSTAR is defined as:

$$\xi = \frac{L_{\text{ion}}}{nR^2} \quad (3)$$

and has units erg cm s^{-1} where L_{ion} is the ionising luminosity from 1 to 1 000 Rydbergs, n is the gas density in cm^{-3} and R is the radius of the absorbing / emitting material from the central source of X-rays. Combining this with the column density which is given by:

$$N_{\text{H}} = \int_{R_{\text{in}}}^{\infty} n dR \quad (4)$$

yields an estimate on the inner radius of the emitting material:

$$R_{\text{in}} \sim \frac{L_{\text{ion}}}{N_{\text{H}}\xi}. \quad (5)$$

Assuming values of $L_{\text{ion}} \sim 5 \times 10^{42} \text{ erg s}^{-1}$ (derived above), $\xi \sim 5000$ and $N_{\text{H}} \sim 3 \times 10^{23} \text{ cm}^{-2}$ then gives a lower limit on R of $\sim 3 \times 10^{15} \text{ cm}$ corresponding to a value of $\sim 200 R_{\text{g}}$ (assuming a black hole mass of $10^8 M_{\odot}$; Nelson & Whittle 1995) and infers an electron density of $n_e \sim 10^8 \text{ cm}^{-3}$ (equation 3). This radius is also consistent with the FWHM of $\sim 10\,000 \text{ km s}^{-1}$ of the H-like Fe line which, if the broadening is assumed to be the intrinsic broadening due to a Keplerian orbit, provides an estimate on the line emitting radius of a few $10^3 R_{\text{g}}$.

4.3 NGC 7213 as a Low Luminosity AGN

4.3.1 The Inner Advective Flow in NGC 7213

From 2–10 keV, the X-ray spectrum of NGC 7213 resembles that of a typical Type 1 Seyfert Galaxy where the spectrum is dominated by a power-law continuum of $\Gamma = 1.75$ and near-neutral Fe K α emission at 6.39 keV. This neutral K α emission may originate from Compton-thin material of $N_{\text{H}} \sim 3 - 4 \times 10^{23} \text{ cm}^{-2}$ possibly in the outer BLR or a Compton-thin torus (Bianchi et al. 2008). We also detect significant emission from highly ionised material located close to the central source with Fe XXV and Fe XXVI perhaps originating in a photo-ionised medium with a column density $N_{\text{H}} \gtrsim 3 \times 10^{23} \text{ cm}^{-2}$ invoked to match the high observed EW of $\sim 60 \text{ eV}$. This emission is likely to originate at a distance of $R \sim 10^3 - 10^4 R_{\text{g}}$ from the black hole / X-ray source.

Given the tight constraints on reflection from both neutral and ionised material ($R < 0.16$ and $R < 0.06$ respectively), the lack of any relativistic signatures and the very weak Big Blue Bump (Wu et al. 1983; often interpreted as thermal emission from the disc), this appears to rule out the presence of an inner, ‘classic’ optically thick, geometrically thin accretion disc (Shakura & Sunyaev 1973) envisaged in the unification scheme of AGN (Antonucci 1993). Instead, we suggest that the accretion disc is maybe truncated at some radius on the order of $10^3 - 10^4 R_{\text{g}}$ ($\sim 0.01 \text{ pc}$) with the inner regions perhaps replaced by a Radiatively Inefficient Accretion Flow (RIAF; Narayan & Yi 1995) consisting of highly ionised, low

density ($n \sim 10^6 \text{ cm}^{-3}$), Compton-thin gas covering some significant fraction of $4\pi \text{ sr}$. In this scenario, the low accretion rate of the source ($0.07\% L_{\text{Edd}}$), perhaps due to a lack of available accreting material, may not allow the infalling material to cool sufficiently in order for a standard thin accretion disc to form. Instead, a stable accretion flow can still occur if the material takes on the form of an optically-thin, hot corona, where most of the material is advected across the event horizon as opposed to radiating away the energy it has acquired in moving close to the black hole.

Such a hot, inner flow is expected to comprise of a low-density plasma whereby collisional processes dominate over photo-ionisation due to the high temperature. At radii below about $100 R_{\text{g}}$, the ion and electron temperatures diverge forming a two-temperature medium with $T_e \sim 10^9 - 10^{10} \text{ K}$ and T_{ion} approaching 10^{12} K in the innermost regions (Narayan & Yi 1995). The electron temperature T_e is then expected to fall as $10^{12} \text{ (K)}/R$ for $R > 10^2$, where R is in Schwarzschild units. However, further out at $R \sim 10^3 - 10^4 R_{\text{S}}$, a plasma temperature of a few 10^8 K (i.e., $k_{\text{B}}T \sim 13 \text{ keV}$, as observed in the collisional APEC model), corresponding to $R \sim 10^4 R_{\text{S}}$, would produce emission from both He-like and H-like Fe, as observed. However, while the Fe XXVI emission could plausibly originate in such a plasma, the presence of the Fe XXV forbidden line suggests that the He-like Fe cannot be solely produced in such a collisionally-ionised medium. Thus an alternative picture could instead be that both the Fe XXV and Fe XXVI emission lines originate in photo-ionised gas, perhaps at the transition region between the RIAF and the cold, outer accretion disc at a radius $R \sim 10^3 - 10^4 R_{\text{g}}$ from the black hole. Alternatively, the Fe XXV / XXVI emission lines may arise from a hybrid of photo- and collisionally-ionised processes.

4.3.2 NGC 7213 as a Low/Hard State Source

The accretion rate of NGC 7213 is much lower than the predicted ‘critical’ value of $\sim 2\% L_{\text{Edd}}$ (Maccarone 2003) whereby the high/soft state in X-ray binaries can be observed. As a result, one interesting possibility is that NGC 7213 is an AGN analogue of the low/hard state observed in Galactic Black Hole Candidates (GBHCs). Long-term monitoring of NGC 7213 with RXTE (Phil Uttley, priv. comm.) shows that the AGN is only slowly variable, indicating a relatively low frequency PSD break. This would be consistent with NGC 7213 having a relatively high black hole mass (e.g., $M_{\text{BH}} = 10^8 M_{\odot}$; Nelson & Whittle 1995; Woo & Urry 2002) but a low accretion rate compared to Eddington, consistent with the scaling relations in the timing properties seen between AGN and GBHCs (McHardy et al. 2006). This is further supported by the SED of NGC 7213 which suggests that this object has interesting radio properties lying between those of Radio-Loud and Radio-Quiet Quasars. Indeed, taking the 5 GHz radio flux and B band flux (host galaxy-subtracted) of Sadler (1984) and Halpern & Filippenko (1984) respectively and using the equation for radio-loudness⁶ of Wilkes & Elvis (1986) gives a value of $R_{\text{L}} \sim 2$ suggesting that NGC 7213 is intermediate between Radio-Quiet AGN and Radio-Loud AGN such as Radio-Galaxies and Blazars. However, Panessa et al. (2007) also find that a radio-loudness of ~ 2 is

⁶ $R_{\text{L}} = \log_{10}(F_{5 \text{ GHz}}/F_{\text{B}})$, where $F_{5 \text{ GHz}}$ and F_{B} are the 5 GHz and B band fluxes respectively. Typically, a value of $R_{\text{L}} \geq 1$ signifies a Radio-Loud object.

not so uncommon in Seyfert galaxies.

The inability to constrain the high energy cutoff of the X-ray emission (i.e., >350 keV) could indicate that the continuum emission may be of non-thermal origin with one possibility being that some of the hard X-ray emission that we observe with *Suzaku* originates from the base of a jet⁷. Hameed et al. (2001) imaged NGC 7213 in the optical band and discovered a giant H α filament approximately 19 kpc from the nucleus. They suggest that such a filament could be the signature of neutral gas shock-ionised by the interactions of a jet. A more recent 8.4 GHz Long Baseline Array (LBA) radio study of NGC 7213 (Blank et al. 2005) reports that the source is unresolved on the scale of ~ 3 milli-arcseconds (corresponding to $\sim 10^4 R_S$ at the distance and black hole mass of NGC 7213), just showing a core, indicating that the jet could be orientated face-on. At lower frequencies, there is also evidence for a large-scale structure (30–40''); Blank, Harnett & Jones 2005 and reference therein) which could possibly be a signature of the extended radio lobes. Consequently, NGC 7213 is perhaps consistent with the hypothesis of Falcke et al. (1996) whereby the radio-intermediate objects are similar to Radio-Quiet AGN but with moderate beaming from pc-scale jets orientated face-on to the observer.

4.3.3 The Origin of the High Energy Continuum

NGC 7213 is not detected to date with the *Fermi* LAT gamma-ray instrument at \sim GeV energies (Abdo et al. 2010) where the inverse-Compton emission from the jet would be expected to dominate. The *Fermi* LAT flux limit corresponding to the detection threshold of Abdo et al. (2010) at the Galactic co-ordinates of NGC 7213 and for $\Gamma = 1.75$ is $F_{0.1-100 \text{ GeV}} < 3 \times 10^{-9}$ photons $\text{cm}^{-2} \text{s}^{-1}$. Extrapolating our best-fit broad-band *Suzaku* model to GeV energies over-predicts the γ -ray flux by a factor of $\sim \times 100$ returning a predicted photon flux of $F_{0.1-100 \text{ GeV}} \sim 3 \times 10^{-7}$ photons $\text{cm}^{-2} \text{s}^{-1}$. This implies that the X-ray continuum does in fact roll over at energies >350 keV.

In order to be consistent with the 0.1–100 GeV flux limit from *Fermi*, we require that the E-folding energy of the power-law component must be $E_{\text{cut}} < 25$ MeV. This, combined with the lower limit on the high-energy cutoff from the combined *Suzaku* / *Swift* data means that $350 \text{ keV} < E_{\text{cut}} < 25 \text{ MeV}$, consistent with the predicted electron temperature of the hot, inner flow (see Section 4.3.1). This suggests that thermal Comptonisation is responsible for the X-ray continuum and that any non-thermal contribution from the inverse-Compton component associated with a jet may be negligible in this source.

Furthermore, the high EW of the observed emission lines may also suggest that there is very little dilution of the X-ray continuum by a jet. We note that other radio-loud sources such as the Broad-Line Radio Galaxies (BLRG) 3C 120 and 3C 390.3 do also show fairly strong Fe K line emission with EWs on the order of 50–100 eV. However, in the case of 3C 390.3, Sambruna et al. (2009) argue from the *Suzaku* data and the overall radio - γ -ray SED that

the jet makes a minimal contribution to the X-ray continuum emission. Likewise, Kataoka et al. (2007) argue a similar case from the *Suzaku* observation of 3C 120 and conclude that the putative jet component does not dilute the Fe K emission. In addition, comparing the ratio of the 1–100 GeV γ -ray flux from *Fermi* to the 2–10 keV X-ray flux for NGC 7213 with that of 3C 111 (the only BLRG detected by *Fermi* to date) and 3C 273, we find that the ratio is higher by a factor of $> \times 6$ for the two radio-loud AGN. By comparison, like for NGC 7213, none of the X-ray bright Type 1 Seyferts appear to have been detected with *Fermi* thus far.

As a further test, we did attempt to model the X-ray continuum with a double power-law component consisting of a hard spectrum to model any possible emission from a jet and a much softer, Seyfert-like spectrum to model the photo-ionising nuclear X-ray emission. Statistically speaking, this fit is not required by the data as it only yields an improvement of $\Delta\chi^2 \sim 2$ for an additional two parameters of interest. Upon fixing the photon index of the softer power-law at $\Gamma = 2$, we find that the normalisation of this component becomes very small with an upper-limit corresponding to just 10% of the normalisation of the main power-law. So it seems that a double power-law model is not required by the data and that the X-ray continuum is best represented by a single power-law component.

The photon index of the X-ray continuum has a best-fit value of $\Gamma = 1.75 \pm 0.02$ and therefore has only a slightly flatter spectrum than the typical values usually associated with Radio-Quiet Quasars (RQQs) and Type 1 Seyferts. For example, Reeves & Turner (2000) find a mean value of $\Gamma = 1.89 \pm 0.05$ from a sample of 27 RQQs observed with *ASCA* (Advanced Satellite for Cosmology and Astrophysics) and Nandra & Pounds (1994) find a mean value of $\Gamma = 1.95$ with a dispersion of $\sigma = 0.15$ from their sample of Seyfert galaxies observed with *Ginga*. Porquet et al. (2004) also find a mean value of $\Gamma = 1.90$ with a dispersion of $\sigma = 0.27$ from a sample of 14 RQQs observed with *XMM-Newton*. The photon index of NGC 7213 is, however, consistent with those found in other low-luminosity AGN such as M81 (Young et al. 2007) and NGC 4579 (Dewangan et al. 2004). Interestingly, the spectrum in NGC 7213 does appear to be somewhat steeper than the predicted photon index of $\Gamma = 1.4$ from the relation between mass accretion rate and photon index of Papadakis et al. (2009) given its calculated accretion rate of 0.07% L_{EDD} (an accretion rate of $\sim 2\%$ L_{EDD} would be required to obtain $\Gamma = 1.75$). So it seems that NGC 7213 may not strictly follow the positive correlation between spectral steepness and accretion rate in AGN and X-ray Binaries suggested by Shemmer et al. (2006) although the high energy cutoff of the X-ray continuum (i.e., $350 \text{ keV} < E_{\text{cut}} < 25 \text{ MeV}$) observed here may suggest that the hard X-ray emission that we observe with *Suzaku* and *Swift* could be consistent with a very hot inner-flow, compatible with NGC 7213 having a low mass accretion rate.

5 CONCLUSIONS

NGC 7213 is an unusual AGN as it consistently exhibits no evidence for a Compton reflection component unlike in other Type 1 Seyferts (Perola et al. 2002; Dadina 2008). The time-averaged continuum emission is well fitted by a single power-law of $\Gamma = 1.75$ and from consideration of the combined *Suzaku* and *Swift* BAT data and the *Fermi* flux limit we constrain the high energy cutoff to be $350 \text{ keV} < E_{\text{cut}} < 25 \text{ MeV}$. The limits on reflection for the neu-

⁷ Note that the high energy cutoff was measured with *BeppoSAX* in 2001 to be $E_{\text{cut}} = 90^{+50}_{-20}$ keV (Bianchi et al. 2004). However, we find no evidence for a cutoff energy < 350 keV with our combined *Suzaku* XIS, HXD and *Swift* BAT spectra.

tral and ionised cases from the REFLIONX model are $R < 0.16$ and $R < 0.06$ respectively suggesting that a significant Compton-thick reflector (e.g., from the inner disc or Compton-thick torus) is absent in this source, consistent with previous findings (e.g., Bianchi et al. 2003). Nonetheless, a significant Fe K complex is observed above 6 keV appearing only in emission. The line from neutral K α dominates (6.39 keV; EW ~ 80 eV) with further contributions from Fe XXV and Fe XXVI Ly α (6.60 and 6.95 keV respectively; also see Starling et al. 2005, Bianchi et al. 2008). Furthermore, in this observation we also find that the Fe XXVI Ly α emission appears to be somewhat resolved in the *Suzaku* spectrum with a FWHM $\sim 10\,000\text{ km s}^{-1}$ and that the emission from Fe XXV appears to be consistent with the forbidden transition from helium-like iron at ~ 6.64 keV as opposed to the resonance transition at ~ 6.70 keV.

The neutral K α emission cannot be modelled via reflection off Compton-thick matter. However, an origin in a Compton-thin plasma covering a significant fraction of 4π sr is feasible with an inferred column density of $N_{\text{H}} \sim 3\text{--}4 \times 10^{23}\text{ cm}^{-2}$, again consistent with the findings of previous observations with *Chandra* and *XMM-Newton*. Likewise here, the emission from highly ionised iron can also be modelled with a substantial column ($N_{\text{H}} \gtrsim 3 \times 10^{23}\text{ cm}^{-2}$) of photo-ionised matter if a location close to the central engine is invoked to explain the inherent broadening and the high ionisation state. Given the lack of either neutral or ionised reflection coupled with the apparent absence of any relativistic signature in the spectrum, it appears that an inner, optically-thick accretion disc may be absent in this source. Instead, the accretion disc in NGC 7213 is most likely truncated at some radius with the inner regions perhaps replaced by an advective accretion flow (e.g., RIAF; Narayan & Yi 1995). The Fe XXV / XXVI emission could then be the ionised signature of such a hot, optically-thin plasma originating in material a few $10^3 R_{\text{g}}$ from the central X-ray source.

6 ACKNOWLEDGEMENTS

This research has made use of the NASA Astronomical Data System (ADS), the NASA Extragalactic Database (NED) and data obtained from the *Suzaku* satellite, a collaborative mission between the space agencies of Japan (JAXA) and the USA (NASA). We wish to thank our anonymous referee for their useful comments and thorough review of the draft. Valentina Braitto would also like to acknowledge support from the UK STFC research council.

REFERENCES

- Abdo A.A., Ackermann M., Ajello M., et al., 2010, preprint (astro-ph/1002.0150v1)
- Anders E., Ebihara M., 1982, *Geochimica et Cosmochimica Acta*, 46, 2363
- Anders E., Grevesse N., 1989, *Geochimica et Cosmochimica Acta*, 53, 197
- Antonucci R., 1993, *ARA&A*, 31, 473
- Arnaud K.A., 1996, in *ASP Conf. Ser. 101: Astronomical Data Analysis Software and Systems V*, ed. G.H. Jacoby & J. Barnes, 17
- Bautista M.A., Kallman T.R., 2000, *ApJ*, 544, 581
- Bianchi S., Matt G., 2002, *A&A*, 387, 76
- Bianchi S., Matt G., Balestra I., Perola G.C., 2003, *A&A*, 407, L21
- Bianchi S., Matt G., Balestra I., Guainazzi M., Perola G.C., 2004, *A&A*, 422, 65
- Bianchi S., Matt G., Nicastro F., Porquet D., Dubau J., 2005, *MNRAS*, 357, 599
- Bianchi S., La Franca F., Matt G., Guainazzi M., Jiménez-Bailón E., Longinotti A.L., Nicastro F., Pentericci L., 2008, *MNRAS*, 389, L52
- Blank D.L., Harnett J.I., Jones P.A., 2005, *MNRAS*, 356, 734
- Boldt E., 1987, *Phys.Rep.*, 146, 215
- Brinkman A.C., Kaastra J.S., van der Meer R.L.J., et al., 2002, *A&A*, 396, 761
- Churazov E., Sunyaev R., Revnivtsev M., 2007, *A&A*, 467, 529
- Dadina M., 2008, *A&A*, 485, 417
- Dewangan G.C., Griffiths R.E., Di Matteo T., Schurch N.J., 2004, *ApJ*, 607, 788
- Dickey J.M., Lockman F.J., 1990, *ARA&A*, 28, 215
- Fabian A.C., Rees M.J., Stella L., White N.E., 1989, *MNRAS*, 238, 729
- Falcke H., Patnaik A.R., Sherwood W., 1996, *ApJ*, 473, L13
- Filippenko A.V., Halpern J.P., 1984, *ApJ*, 285, 458
- Fukazawa Y., Mizuno T., Watanabe S., et al., 2009, *PASJ*, 61, 17
- George I.M., Fabian A.C., 1991, *MNRAS*, 249, 352
- Grevesse N., Noels A., Sauval A.J., 1996, *ASPC*, 99, 117
- Gruber D.E., Matteson J.L., Peterson L.E., Jung G.V., 1999, *ApJ*, 520, 124
- Halpern J.P., Filippenko A.V., 1984, *ApJ*, 285, 475
- Hameed S., Blank D.L., Young L.M., Devereux N., 2001, *ApJ*, 546, 97
- Ho L.C., 1999, *ApJ*, 516, 672
- Ishida M., Suzuki K., Someya K., 2007, *JX-ISAS-SUZAKU-MEMO-2007-11*
- Ishisaki Y., Maeda Y., Fujimoto R., et al., 2007, *PASJ*, 59, 113
- Kaastra J.S., Mewe R., 1993, *A&AS*, 97, 443
- Kalberla P.M.W., Burton W.B., Hartmann D., Arnal E.M., Bajaja E., Morras R., Pöppel W.G.L., 2005, *A&A*, 440, 775
- Kallman T.R., McCray R., 1982, *ApJ*, 50, 263
- Kaspi S., Brandt W.N., Netzer H. et al., 2001, *ApJ*, 554, 216
- Kataoka J., Reeves J.N., Iwasawa K., 2007, *PASJ*, 59, 279
- Kinkhabwala A., Sako M., Behar E., et al., 2002, *ApJ*, 575, 732
- Kokubun M., Makishima K., Takahashi T., et al., 2007, *PASJ*, 59, 53
- Koyama K., Tsunemi H., Dotani T., et al., 2007, *PASJ*, 59, 23
- Maccarone T.J., 2003, *A&A*, 409, 697
- Magdziarz P., Zdziarski A.A., 1995, *MNRAS*, 273, 837
- Matt G., Perola G.C., Piro L., 1991, *A&A*, 247, 25
- McHardy I.M., Koerding E., Knigge C., Uttley P., Fender R.P., 2006, *Nat*, 444, 730
- Mitsuda K., Bautz M., Inoue H., et al., 2007, *PASJ*, 59, 1
- Morrison R., McCammon D., 1983, *ApJ*, 270, 119
- Mould J., Huchra J.P., Freedman W.L., et al., 2000, *ApJ*, 529, 786
- Murphy K.D., Yaqoob T., 2009, *MNRAS*, 397, 1549
- Nandra K., Pounds K.A., 1994, *MNRAS*, 268, 405
- Narayan R., Yi I., 1995, *ApJ*, 452, 710
- Nelson C.H., Whittle M., 1995, *ApJS*, 99, 67
- Netzer H., Laor A., 1993, *ApJ*, 404, 51
- Padovani P., Rafanelli P., 1988, *A&A*, 205, 53
- Page M.J., 2001, *MNRAS*, 328, 925
- Page M.J., Breeveld A.A., Soria R., et al., 2003, *A&A*, 400, 145
- Panessa F., Barcons X., Bassani L., Cappi M., Carrera F.J., Ho L.C., Pellegrini S., 2007, *A&A*, 467, 519
- Papadakis I.E., Sobolewska M., Arevalo P., Markowitz A., McHardy I.M., Miller L., Reeves J.N., Turner T.J., 2009, *A&A*, 494, 905
- Perola G.C., Matt G., Cappi M., Fiore F., Guainazzi M., Maraschi L., Petrucci P.O., Piro L., 2002, *A&A*, 389, 802
- Porquet D., Dubau J., 2000, *A&AS*, 143, 495
- Porquet D., Reeves J.N., O'Brien P., Brinkmann W., 2004, *A&A*, 422, 85
- Pounds K.A., Page K.L., 2005, *MNRAS*, 360, 1123
- Reeves J.N., Turner T.J., 2000, *MNRAS*, 316, 234
- Ross R.R., Fabian A.C., 2005, *MNRAS*, 358, 211
- Sadler E.M., 1984, *AJ*, 89, 53
- Sambruna R.M., Reeves J.N., Braitto V., et al., 2009, *ApJ*, 700, 1473
- Schurch N.J., Warwick R.S., 2002, *MNRAS*, 334, 811
- Shakura N.I., Sunyaev R.A., 1973, *A&A*, 24, 337
- Shemmer O., Brandt W.N., Netzer H., Maiolino R., Kaspi S., 2006, *ApJ*, 646, 29
- Smith R.K., Brickhouse N.S., Liedahl D.A., Raymond J.C., 2001, 556, L91
- Starling R.L.C., Page M.J., Branduardi-Raymont G., Breeveld A.A., Soria R., Wu K., 2005, *MNRAS*, 356, 727
- Takahashi T., Abe K., Endo M., et al., 2007, *PASJ*, 59, 35

- Tueller J., Baumgartner W.H., Markwardt C.B., et al., 2009, preprint (astro-ph/0903.3037)
- Verner D.A., Ferland G.J., Korista K.T., Yakovlev D.G., 1996, ApJ, 465, 487
- Wandel A., 1999, ApJ, 527, 657
- Wilkes B.J., Elvis M., 1986, BAAS, 18, 925
- Woo J.-H., Urry C.M., 2002, ApJ, 579, 530
- Wu C.-C., Boggess A., Gull T.R., 1983, ApJ, 266, 28
- Yaqoob T., Murphy K.D., Miller L., Turner T.J., 2010, MNRAS, 401, 411
- Young A.J., Nowak M.A., Markoff S., Marshall H.L., Canizares C.R., 2007, ApJ, 669, 830